Applied Catalysis A: General 507 (2015) 56–64

Contents lists available at ScienceDirect

Applied Catalysis A: General

journal homepage: www.elsevier.com/locate/apcata

Methanol oxidative decomposition over zirconia supported silver catalyst and its reaction mechanism

Naohiro Shimoda[a], Shota Umehara[a], Masaki Kasahara[a], Teruhisa Hongo[a,1], Atsushi Yamazaki[b], Shigeo Satokawa[a,*]

[a] Department of Materials and Life Science, Faculty of Science and Technology, Seikei University, 3-3-1 Kichijoji-kitamachi, Musashino-shi, Tokyo 180-8633, Japan

[b] Development of Resources and Envirnmental Engineering, School of Creative Science and Engineering, Waseda University, 3-4-1 Okubo, Shinju-ku, Tokyo 169-8555, Japan

ARTICLE INFO

Article history:
Received 12 June 2015
Received in revised form
10 September 2015
Accepted 11 September 2015
Available online 25 September 2015

Keywords:
Methanol oxidation
Ag catalyst
VOCs
Zirconia
FTIR

ABSTRACT

To develop a new catalyst for catalytic decomposition of volatile organic compounds (VOCs), the activity of various oxide supported silver (Ag) based catalysts for methanol (MeOH) oxidation reaction have been evaluated. Based on the activity evaluation, zirconia (ZrO_2) is considered to be a substitute to ceria (CeO_2) as a support material. The ZrO_2 supported catalyst loading Ag component can oxidize MeOH to CO_2 completely, while the main product is CO for MeOH oxidation over pure ZrO_2. In the present work, 2.0 wt.% Ag/ZrO_2 exhibits excellent activity comparable to Ag/CeO_2. Furthermore, according to *in situ* FT-IR analysis over Ag/ZrO_2 and pure ZrO_2, it is considered that the methoxy, formate, and bicarbonate species adsorbed on the ZrO_2 surface are intermediate species. We thus deduce that Ag component significantly enhances the oxidation step of methoxy species to CO_2 *via* formate species, leading to the complete oxidation of MeOH to CO_2 over Ag/ZrO_2 catalyst.

1. Introduction

Volatile organic compounds (VOCs) are recognized as air pollutants that cause photochemical smog, ground-level ozone, sick house syndrome, and chemical sensitivity [1–4]. Thus, detoxification treatment of VOCs is required and the emission regulation of VOCs is established by Air Pollution Control Act in any countries. Among VOCs, formaldehyde is produced by partial oxidation of methanol (MeOH) and used as organic solvents, coating materials, and resinous raw materials [5]. Various methods: flame combustion, catalytic decomposition using plasma, photocatalytic decomposition, adsorbent-based methods, have been intensively investigated for the effective abatement of VOCs. The catalytic combustion process has advantageous features for VOCs removal as compared with other methods [6]. In the catalytic combustion process, the selection of active metal materials is an important factor for the development of catalysts. Transition metal catalysts are more efficient on a cost basis as compared with precious metal ones; however, the former exhibits lower activity for VOCs combustion [7–9]. On the other hand, precious metal catalysts can achieve the complete oxidation at low temperature due to their high activity [10–13]. For the MeOH oxidative decomposition process, Pt [14], Ru [15,16], Au [17–19], and Ag [20–25] metals have been well researched as active metals. In addition, transition metal based catalysts using the Cu [26–29], Mo [30], Ni [31,32], and V [33–36] metals have been also reported. Cerium oxide (ceria, CeO_2) is considered an attractive support due to its high oxygen storage capacity (OSC) [37,38]. Actually, many researchers reported that ceria supported precious metal catalysts exhibit high activity for formaldehyde, MeOH, and other VOCs oxidation reactions [7,8,13,17,19,24,37,39]. However, the cost of precious metal catalysts and their catalytic degradation will become serious problems for the practical application. Additionally, the supply risk of precious metals and rare-earth metals including cerium is a serious international problem. Thus, several oxides such as TiO_2 [18,40], SiO_2 [26], Al_2O_3 [23,41], ZnO [18,28], FeOx [42], ZrO_2 [15,16,26,29,30], CeO_2–ZrO_2 [14,24], and mesoporous SiO_2 [19,27] have been investigated as support materials and a novel catalyst

* Corresponding author. Fax: +81 422 37 3871.
E-mail address: satokawa@st.seikei.ac.jp (S. Satokawa).
[1] Present address: Work Environment Research Group, National Institute of Occupational Safety and Health, 6-21-1 Nagao, Tama-Ku, Kawasaki 214-8585, Japan.

http://dx.doi.org/10.1016/j.apcata.2015.09.017
0926-860X/

for the oxidation process of MeOH as well as other VOCs have been studied [43].

Based on this background, in the present study, we have focused on a supported silver (Ag) catalyst for the oxidation of MeOH which convert to formaldehyde easily. In particular, we have studied zirconium oxide (zirconia, ZrO_2) supported Ag (Ag/ZrO_2) catalysts, because the ZrO_2 support is considered to be a suitable alternative candidate to CeO_2 and also there is no report of the MeOH oxidative decomposition over Ag/ZrO_2 catalyst. Specifically, the comparative study of the catalytic activity of Ag/ZrO_2 with other several oxide supported metal catalysts for MeOH oxidation has been conducted. Furthermore, *in-situ* Fourier transform infrared spectroscopy (FT-IR) analysis of the catalyst have been undertaken to obtain the insight on the reaction mechanism for MeOH oxidation over Ag/ZrO_2 catalyst.

2. Experimental

2.1. Catalyst preparation

The various metal oxide supported metal catalysts were prepared by the impregnation method [44]. The following metal oxides were used as support materials: ZrO_2 (JRC-ZRO-3 and JRC-ZRO-2), CeO_2 (JRC-CEO-3), MgO (JRC-MGO-4 500A) provided by the Catalysis Society of Japan; MnO_2 (MN-280) provided by Clariant Catalysts (Japan) K.K.; Al_2O_3 prepared from aluminum hydroxides (Catapal B) provided by Sasol Ltd. by the heat treatment in air at 600 °C for 2 h. An aqueous solution of $AgNO_3$ provided by Wako Pure Chemical Industries, Ltd. was used as the Ag source. In addition, $Pt(NH_3)_2(NO_2)_2$ nitric acid solution provided by Kojima Chemical Co., Ltd. and $Co(NO_3)_2$ hexahydrate, $Cu(CH_3COO)_2$ monohydrate, and $SnCl_2$ dihydrate provided by Wako Pure Chemical Industries, Ltd., were used as each metal source. The loading of Ag metal was adjusted to 0.5–5.0 wt.% in the metallic form. Each metal oxide powder was impregnated with an aqueous solution of the metal component of interest. The mixture was stirred at room temperature under 13 kPa for 2 h and then the solution was evaporated sufficiently on a water bath at 80 °C under 40 kPa. The obtained samples were dried in air at 110 °C and then calcined in air at 500 °C for 2 h. Subsequently, the obtained powders were pressed, crushed, and sieved to particle size of 150–250 μm for the catalytic activity tests of MeOH oxidation.

2. 2 Catalytic activity test

The evaluation of catalytic performance for MeOH oxidation was conducted using a fixed-bed flow reactor. The prepared catalyst (0.2 g) was housed in the quartz tube reactor with a diameter of 6 mm and a reaction gas mixture (700 ppm MeOH/20% O_2/He balance) was fed to the catalyst bed at a total flow rate of 300 mL/min (gas hourly space velocity: 100,000 L kg^{-1} h^{-1}). The compositions of the inlet and outlet gases were analyzed using a gas chromatograph equipped with a flame ionization detector (Shimadzu, GC-8A). A SHINCARBON ST 50–80 column (Shinwa Chem. Ind.) and a methanizer accessory were used to determine the amount of MeOH, CO, and CO_2.

2.3. Catalyst characterization

The specific surface area of each support oxide without and with the heat treatments and each prepared catalyst was determined by N_2 adsorption measurement at 77 K by the conventional BET method using a Microtrac BEL BELSORP-mini II instrument. Prior to N_2 adsorption, the sample was degassed at 200 °C for 2 h in order to remove the moisture adsorbed on the surface and inside the porous network.

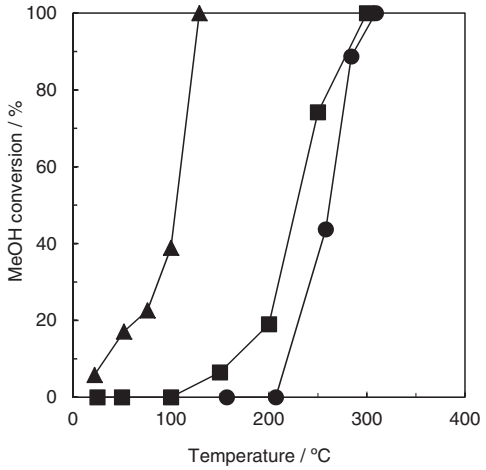

Fig. 1. Catalytic activity of various oxides for MeOH oxidation: (●) ZrO_2 (JRC-ZRO-3), (■) CeO_2, (JRC-CEO-3), (▲) MnO_2 (MN-280); reaction conditions: 700 ppm MeOH/20% O_2/He balance; W/F: 0.04 g h cm^{-3}.

To identify the crystalline structure of each support oxide and each prepared catalyst, the powder X-ray diffraction (XRD) pattern was measured using a Rigaku Ultima IV instrument equipped with a Cu Kα radiation source (λ = 0.154 nm). The typical working conditions such as an acceleration voltage and current were 40 kV and 20 mA with a scanning speed of 1° min^{-1}.

Transmission electron microscopy (TEM) of 2.0 wt.% Ag/ZrO_2 and 2.0 wt.% Ag/CeO_2 was performed using a JEOL JEM-2100F operated at 200 kV. The samples were dispersed by ultrasonic in ethanol followed by deposition of the resultant suspension onto a standard Cu grid covered with a holey carbon film.

To elucidate the adsorbed species and intermediates during MeOH oxidation over pure ZrO_2 and Ag/ZrO_2, *in-situ* Fourier transform infrared spectroscopy (FT-IR) analysis was conducted using a SHIMADZU FTIR-8300 equipped with a glass reaction cell (Makuhari Rikagaku Garasu Inc.). Thin disks of each sample were made and placed in the FT-IR cell. For the measurement of Ag/ZrO_2, the spectrum was recorded under 20% O_2/He at the temperature range of room temperature to 125 °C after the pre-treatments as follows: heat-treatment in 20% O_2/He at 200 °C for 2 h, and then cooling to room temperature. Subsequently, a gaseous mixture of 1% MeOH/20% O_2/He balance was fed the samples to adsorb the MeOH-derived species on the sample surface. The interior of reaction cell was then purged with 20% O_2/He for 15 min. For the measurement of pure ZrO_2, the adsorption step of MeOH was carried out at 200 °C and the spectrum was recorded under 20% O_2/He gaseous condition at the temperature range of 200–300 °C after the pretreatment as mentioned above. For the both measurements, prior to the MeOH adsorption step, back ground spectrum was recorded in 20% O_2/He at room temperature or 200 °C, respectively. The IR measurement was operated at a resolution of 4 cm^{-1}, and 45 scans were collected for each spectrum.

3. Results and discussion

3.1. Catalytic activity for MeOH oxidation

3.1.1. Activity of various oxides

Firstly, the catalytic activity of the representative pure oxides for MeOH oxidative decomposition has been evaluated. Fig. 1 shows the temperature dependence of MeOH conversion for MeOH oxidation over ZrO_2 (JRC-ZRO-3), CeO_2, (JRC-CEO-3), and MnO_2 (MN-280) oxides as-obtained. Among them, pure MnO_2 exhibited much higher activity than ZrO_2 and CeO_2. As shown in Table 1,

Table 1
BET surface area[a] and crystalline phase of various metal oxides.

Metal oxide	Abbreviation	Heat treatment	BET surface area ($m^2\ g^{-1}$)	Crystalline phase
CeO_2 (JRC-CEO-3)	CeO_2	As-obtained	86	Cubic (fluorite)
MnO_2 (MN-280)	MnO_2	As-obtained	222	Tetragonal (rutile)
MgO (JRC-MGO-4 500A)	MgO	As-obtained	36	Cubic
Al_2O_3[b]	Al_2O_3	600 °C	178	Cubic (gamma)
ZrO_2 (JRC-ZRO-3)	ZrO_2	As-obtained	99	Monoclinic
ZrO_2 (JRC-ZRO-2)	$ZrO_2(2)$	As-obtained	227	Amorphus
ZrO_2 (JRC-ZRO-2)	$ZrO_2(2)$ 320	320 °C	191	Amorphus
ZrO_2 (JRC-ZRO-2)	$ZrO_2(2)$ 400	400 °C	102	Monoclinic and tetragonal
ZrO_2 (JRC-ZRO-2)	$ZrO_2(2)$ 800	800 °C	13	Monoclinic and tetragonal

[a] Heat-treated at 200 °C for 2 h in vacuum prior to N_2 adsorption and desorption measurement.
[b] Alumina was prepared by the calcination of AlOOH in air at 600 °C for 2 h.

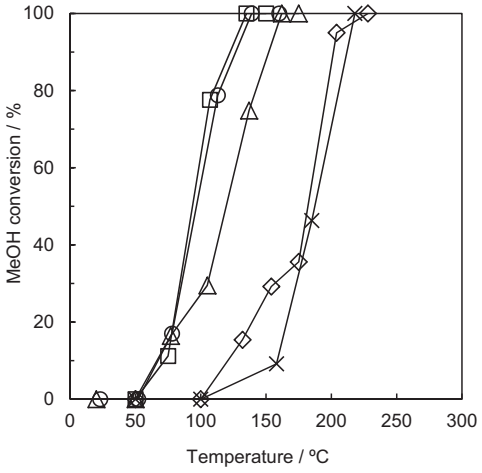

Fig. 2. Catalytic activity of various oxide supported Ag catalysts for MeOH oxidation: (○) Ag/ZrO_2, (□) Ag/CeO_2, (△) Ag/MnO_2, (◇) Ag/MgO, (×) Ag/Al_2O_3; reaction conditions: 700 ppm MeOH/20% O_2/He balance; W/F: 0.04 g h cm^{-3}; metal loading: 2.0 wt.%.

the BET specific surface area of MnO_2 was 104 $m^2\ g^{-1}$ which was higher than those of ZrO_2 (99 $m^2\ g^{-1}$) and CeO_2 (86 $m^2\ g^{-1}$). We have also examined the activity of gamma-Al_2O_3 (178 $m^2\ g^{-1}$) and MgO (36 $m^2\ g^{-1}$) for MeOH oxidation (results are not shown), which resulted in the lower activity. For the MnO_2, ZrO_2, and CeO_2, the complete conversion of MeOH was achieved at 125 °C, 300 °C, and 300 °C, respectively. For the MnO_2 and CeO_2, MeOH was mainly converted to CO_2, meaning the low CO selectivity at the temperature rages where MeOH was oxidized. In particular, MnO_2 can oxidize MeOH to CO_2 completely, whilst main product for MeOH oxidation over ZrO_2 was found to be CO and H_2O as shown in Fig. S1. In the literature, Delimaris and Ioannides reported high CO_2 selectivity for oxidation of ethanol, ethyl acetate, and toluene over MnO_X, CeO_2, and MnO_X–CeO_2 catalysts. It may be considered that MnO_2 and CeO_2 exhibit high activity and high selectivity of CO_2 for the MeOH oxidation reaction. In addition, ZrO_2 showed relatively high performance for the MeOH oxidative decomposition to CO. We thus consider that the important factor contributing to the catalytic performance of metal oxides is not only their surface area but also other physicochemical properties.

Supplementary material related to this article found, in the online version, at http://dx.doi.org/10.1016/j.apcata.2015.09.017.

3.1.2. *Effect of the precious metal loading upon the various oxides*

To improve the catalytic activity accompanying complete oxidation for MeOH oxidation, we have studied the effect of Ag loading. Fig. 2 shows the MeOH conversions for MeOH oxidation over various oxide supported Ag catalysts with 2.0 wt.% loading. The temperatures at which MeOH was converted completely were

Table 2
BET surface area[a] of various metal oxide supported Ag catalysts.[b]

Metal oxide	Final calcination temperature	BET surface area ($m^2\ g^{-1}$)
CeO_2	500 °C	74
MnO_2	500 °C	104
MgO	500 °C	104
Al_2O_3	500 °C	176
ZrO_2	500 °C	62
$ZrO_2(2)$	110 °C	191
$ZrO_2(2)$ 320	320 °C	178
$ZrO_2(2)$ 400	400 °C	87
$ZrO_2(2)$ 800	500 °C	15

[a] Heat-treated at 200 °C for 2 h in vacuum prior to N_2 adsorption and desorption measurement.
[b] Ag loading: 2.0 wt.%.

230 °C, 220 °C, 160 °C, 140 °C, and 135 °C for the MgO, Al_2O_3, MnO_2, ZrO_2 (JRC-ZRO-3), and CeO_2 supported Ag catalysts, respectively. The Ag/ZrO_2, Ag/CeO_2 and Ag/MnO_2 exhibited higher activity than those of the other catalysts. In particular, 2.0 wt.% Ag/ZrO_2 exhibited excellent activity comparable to 2.0 wt.% Ag/CeO_2. At the low conversion region, 2.0 wt.% Ag/MnO_2 exhibited high conversion of MeOH; however, Ag loading negatively affected MeOH oxidation compared with the catalytic activity of pure MnO_2. In contrast, for the ZrO_2 and CeO_2 catalysts, the loading of Ag component on each oxide was significantly improved catalytic activity. Furthermore, it was found that the product was only CO_2 and H_2O over all Ag-based catalysts. This indicates that the oxide supported Ag catalysts can oxidize MeOH to CO_2 completely due to the facilitative effect of Ag element for CO oxidation step. As shown in Table 2, the BET specific

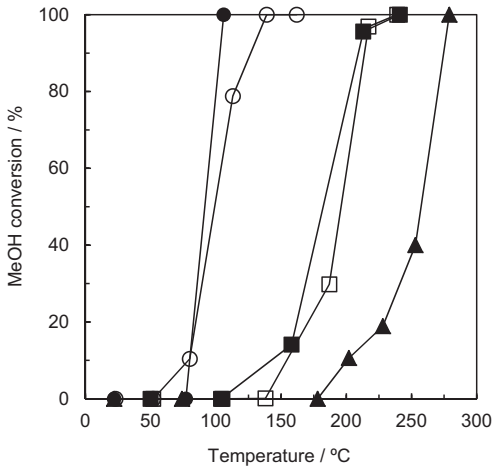

Fig. 3. Catalytic activity of zirconia (JRC-ZRO-3) supported various metal catalysts for MeOH oxidation: (○) Ag/ZrO_2, (●) Pt/ZrO_2, (■) Co/ZrO_2, (□) Cu/ZrO_2, (▲) Sn/ZrO_2; reaction conditions: 700 ppm MeOH/20% O_2/He balance; W/F: 0.04 g h cm^{-3}; metal loading: 2.0 wt.%.

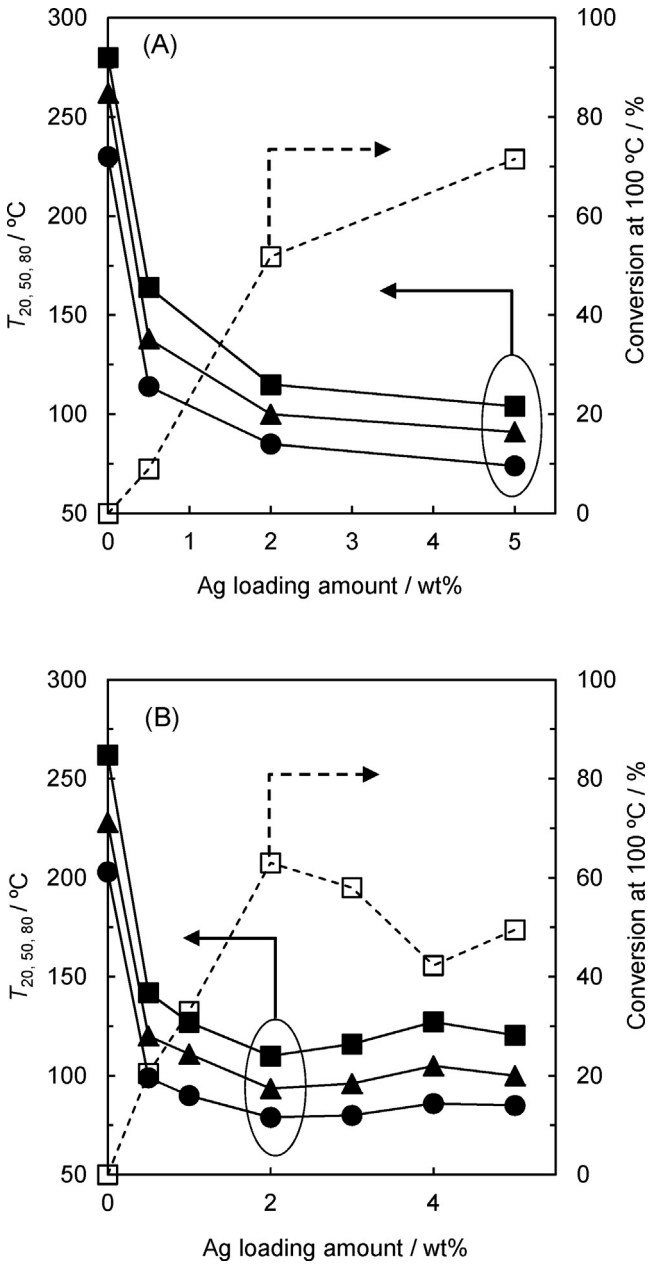

Fig. 4. Effect of Ag loading of (A) zirconia and (B) ceria supported Ag catalysts on the activity for MeOH oxidation: (closed symbol) reaction temperatures to achieve the conversion of 20% (T_{20}, ●), 50% (T_{50}, ▲), 80% (T_{80}, ■); (open symbol, □) conversion at 100 °C; reaction conditions: 700 ppm MeOH/20% O_2/He balance; W/F: 0.04 g h cm^{-3}.

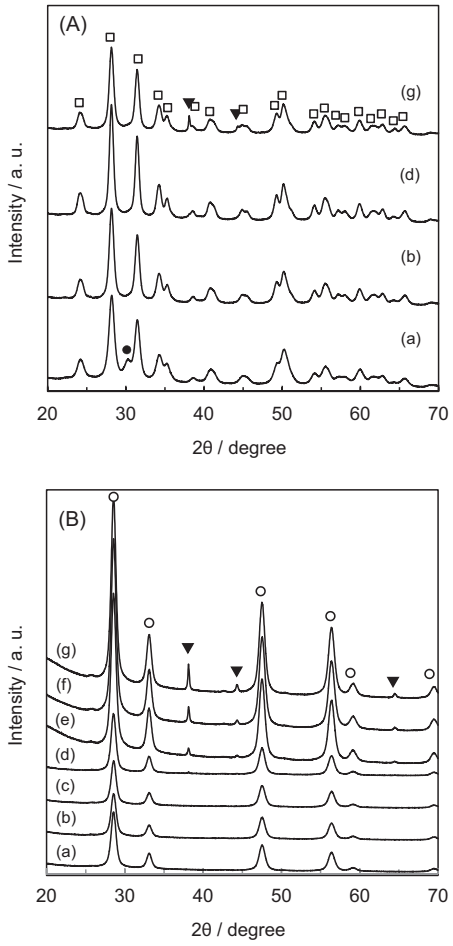

Fig. 5. XRD patterns of (A) zirconia and (B) ceria supported Ag catalysts with various loading: (a) 0 wt.%, (b) 0.5 wt.%, (c) 1.0 wt.%, (d) 2.0 wt.%, (e) 3.0 wt.%, (f) 4.0 wt.%, (g) 5.0 wt.%; (□) ZrO_2-monoclinic, (●) ZrO_2-tetragonal, (▼) Ag, (○) CeO_2-cubic.

surface areas of the supported Ag catalysts were lower than those of all metal oxides except MgO (104 $m^2 g^{-1}$). The difference between pure MnO_2 (222 $m^2 g^{-1}$) and Ag/MnO_2 (104 $m^2 g^{-1}$) was particularly large among the catalysts. This may be the reason why the final calcination during the Ag loading decreased the BET specific surface area of MnO_2. Based on the XRD analysis, the pure MgO as-obtained (JRC-MGO-4 500 A) included a fixed content of $Mg(OH)_2$. We consider that the heat treatment in air at 500 °C in the procedure of Ag loading resulted in the formation of pure MgO, leading to an increase in the BET specific surface area of Ag/MgO.

3.1.3. Zirconia supported precious metal catalysts

Next, we have studied the effect of active metal species for MeOH oxidation over zirconia supported catalysts. The MeOH conversion over zirconia supported 2.0 wt.% metal catalysts for MeOH oxidation are shown in Fig. 3. Over Pt/ZrO_2, MeOH oxidation abruptly occurred at 75 °C. It is well known that CO can be strongly adsorbed on Pt. The adsorption amount of CO on Pt is higher than those on other metal catalysts and may be considered dependent upon the temperature. Therefore, it is presumed that the adsorption of formed CO is more dominant than the progress of CO oxidation reaction at low temperature. We suppose that this may be one of the reasons that the steep activation behavior for MeOH oxidation over Pt/ZrO_2. In addition, Ag/ZrO_2 catalyst exhibited the comparable high activity. However, Co, Cu, and Sn/ZrO_2 catalysts showed low activity. We consider that this reason may be due to their low activity for the CO oxidation step.

3.2. Comparison of the activity of Ag/ZrO_2 and Ag/CeO_2 catalysts

As mentioned above, 2.0 wt.% Ag/ZrO_2 exhibits an excellent activity which is comparable to 2.0 wt.% Ag/CeO_2. Hence, we have studied the effect of loadings of Ag on Ag/ZrO_2 and Ag/CeO_2 for MeOH oxidation. Fig. 4 presents the activity of both catalysts with various loadings of Ag. The reaction temperature to achieve a MeOH conversion of 20%, 50%, and 80% for MeOH oxidation and the MeOH conversion at 100 °C are plotted in Fig. 4. From these results, the optimum amounts of silver loading for zirconia and ceria catalysts were found to be 5.0 wt.% and 2.0 wt.%, respectively.

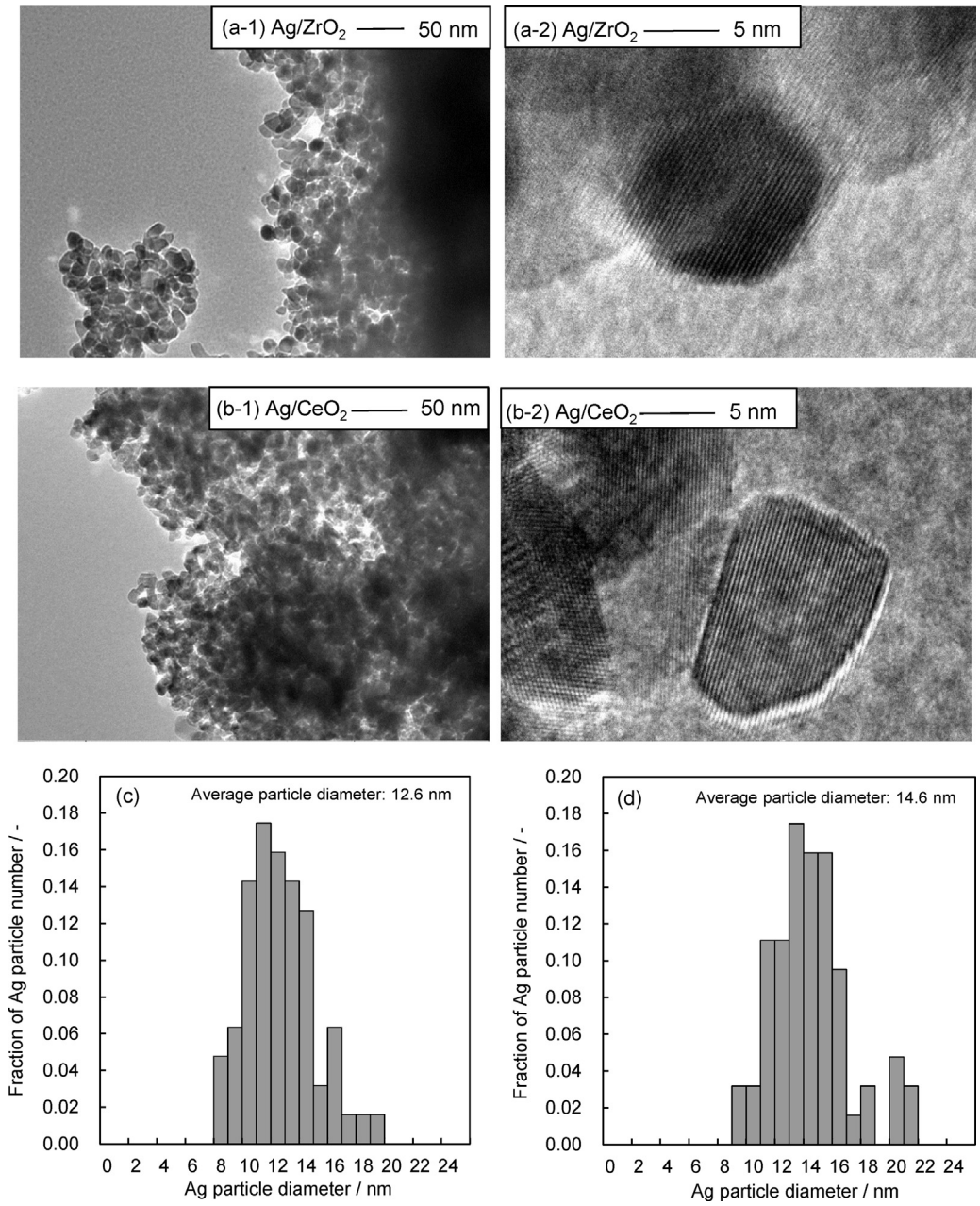

Fig. 6. TEM images and Ag particle size distribution of (a, c) 2.0 wt.% Ag/ZrO_2 (JRC-ZRO-3) and (b, d) 2.0 wt.% Ag/CeO_2 (JRC-CEO-3) catalysts after the activity tests of MeOH oxidation shown in Fig. 2.

Fig. 5 shows the XRD patterns of Ag/ZrO_2 and Ag/CeO_2 catalysts with various loadings. The main crystalline phase of support oxide for both catalysts were monoclinic zirconia and cubic ceria, respectively. The diffraction peaks attributed to Ag component were observed for the catalyst with the loading amount above 2.0 wt.%. The crystallinity of the Ag phase for Ag/CeO_2 were higher than for Ag/ZrO_2. Furthermore, TEM observation of 2.0 wt.% Ag/ZrO_2 and 2.0 wt.% Ag/CeO_2 was conducted as shown in Fig. 6. The average particle sizes of silver metal for both catalysts were approximately 12.6 nm and 14.6 nm, respectively. As shown in Table 2, the BET surface areas of 2.0 wt.% Ag/ZrO_2 and 2.0 wt.% Ag/CeO_2 were 62 $m^2\,g^{-1}$ and 74 $m^2\,g^{-1}$, respectively. We consider that the loading of Ag on both oxides enhances the catalytic activity for MeOH oxidation with the same level of positive effect. For the catalytic combustion reaction, the BET surface area of the oxide is an important factor for the activity of catalyst [6–8]. In the present work, the difference of BET surface area between the 2.0 wt.% Ag/ZrO_2 and 2.0 wt.% Ag/CeO_2 was 12 $m^2\,g^{-1}$. Thus, we consider that this difference is negligible for the comparison of both catalysts.

3.3. *Effect of ZrO_2 type on the catalytic activity of Ag/ZrO_2 catalyst for MeOH oxidation*

Next, we have examined the effect of zirconia surface area and crystallinity on the catalytic activity for various Ag/ZrO_2 materials. The physical properties of various ZrO_2 and ZrO_2 supported Ag catalysts are summarized in Tables 1 and 2, respectively. Two types ZrO_2 were used in the present work and abbreviated as $ZrO_2(2)$ and ZrO_2 which is the ZrO_2 (JRC-ZRO-3). The crystalline phases of pure $ZrO_2(2)$ and ZrO_2 samples as obtained were amorphous and monoclinic and their BET surface areas were 227 $m^2\,g^{-1}$ and 99 $m^2\,g^{-1}$, respectively. Additionally, $ZrO_2(2)X$ samples produced

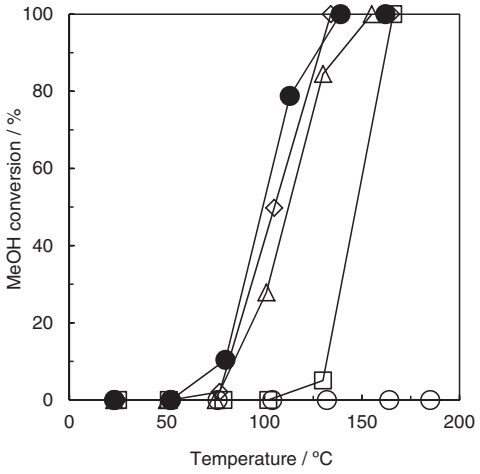

Fig. 7. Catalytic activity of various zirconia supported Ag catalysts for MeOH oxidation: (●) ZrO_2, (○) ZrO_2(2), (□) ZrO_2(2) 320, (◊) ZrO_2(2) 400, (△) ZrO_2(2) 800; reaction conditions: 700 ppm MeOH/20% O_2/He balance; W/F: 0.04 g h cm^{-3}; metal loading: 2.0 wt.%.

by the heat treatment in air at 320 °C, 400 °C, 800 °C (*X* denotes the temperature of treatment) were used as support oxides and the final calcination temperatures after the loading of Ag were same as each heat treatment temperature. With an increase in the temperature of heat treatment, the BET surface area of ZrO_2(2) decreased and the crystallite phase varied from amorphous to polymorphism phase of monoclinic and tetragonal.

Fig. 7 shows the activity of these Ag/ZrO_2 catalysts for MeOH oxidation. Among the ZrO_2(2) supported Ag catalysts, the Ag/ZrO_2(2) exhibited no activity for oxidation below 200 °C. In contrast, the activity of Ag/ZrO_2(2) 400 exhibited high activity, which was comparable to the activity for Ag/ZrO_2. In addition, we unexpectedly found that the Ag/ZrO_2(2) 800 possessed higher activity than Ag/ZrO_2(2) 320. The BET surface areas of Ag/ZrO_2(2)*X* with the heat treatment at 320 °C, 400 °C, and 800 °C were 178 m^2 g^{-1}, 87 m^2 g^{-1}, 15 m^2 g^{-1}, respectively. Considering the difference of the activity between the catalysts using ZrO_2(2) 320 and ZrO_2(2) 400 of which crystalline phases were amorphous as shown in Table 1, it is found that the crystallization of zirconia affect the activity of catalyst significantly. This may be because the low mobility of lattice oxygen in the zirconia with the low crystallinity results in the low activity of zirconia for MeOH oxidation. Indeed, in the present work, the monoclinic ZrO_2 supported Ag catalysts exhibited high activity. In addition, we consider that the larger BET surface area of zirconia leads to the higher catalytic activity of Ag/ZrO_2 by comparing the activity of the catalysts with the heat treatment at 400 °C and 800 °C. However, it is worth noting that the effect of the BET surface area of support oxides was less important than that of crystallinity of support oxides for MeOH oxidation over Ag/ZrO_2.

3.4. *FT-IR analysis on MeOH oxidation over pure ZrO_2 and Ag/ZrO_2 catalysts*

To obtain insight into the reaction mechanism of MeOH oxidation over Ag/ZrO_2, we have conducted *in situ* FT-IR analysis. Firstly, we have examined the adsorbed species on the pure ZrO_2 (JRC-ZRO-3), as shown in Fig. 8. It should be noted that the FT-IR analysis was carried out from 200 °C to 300 °C for the pure ZrO_2. After MeOH was adsorbed at 200 °C, two inverse bands at 3725 cm^{-1} and 3670 cm^{-1} were observed. These bands are assigned to hydroxyl (OH) groups on ZrO_2, including terminal (higher) and bridging (lower) types. In addition, several adsorption bands appeared at 2920 cm^{-1}, 2810 cm^{-1}, and 1195 cm^{-1}, and also appeared at 2870 cm^{-1}, 1575 cm^{-1}, 1385 cm^{-1}, and 1360 cm^{-1}; they were assigned to methoxy (CH_3) groups and formate (HCOO) groups, respectively. The bands associated with bicarbonate (HCO_3) groups was also observed at 1421 cm^{-1}. These results indicate a decrease of the hydroxyl groups due to the adsorption of MeOH with the replacement of the hydroxyl species on the ZrO_2 surface. When the measurement temperature was increased, the adsorption bands of methoxy species decreased but those of formate and bicarbonate bands increased. We consider that this proves the progress of transformation of methoxy species to formate and bicarbonate species. After the further increases in the measurement temperature, a decrease in the inverse bands of the hydroxyl groups was apparently observed. We consider that this implies the regeneration of the hydroxyl groups on the ZrO_2 surface, indicating the oxidation of formate species to CO and the hydroxyl species. Dur-

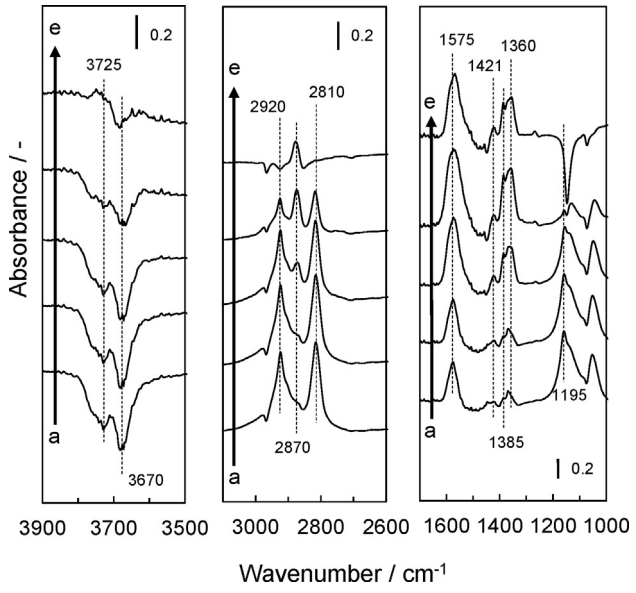

Fig. 8. *In situ* FT-IR spectra of adsorbed species on pure ZrO_2 (JRC-ZRO-3) for MeOH oxidation upon increasing temperature: (a) 200 °C, (b) 225 °C, (c) 250 °C, (d) 275 °C, (e) 300 °C.

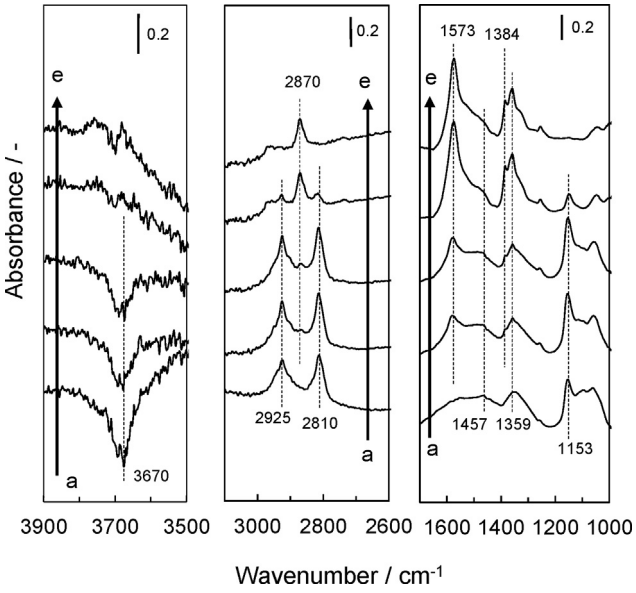

Fig. 9. *In situ* FT-IR spectra of adsorbed species on 2.0 wt.% Ag/ZrO_2 (JRC-ZRO-3) for MeOH oxidation upon increasing temperature: (a) room temperature, (b) 50 °C, (c) 75 °C, (d) 100 °C, (e) 125 °C.

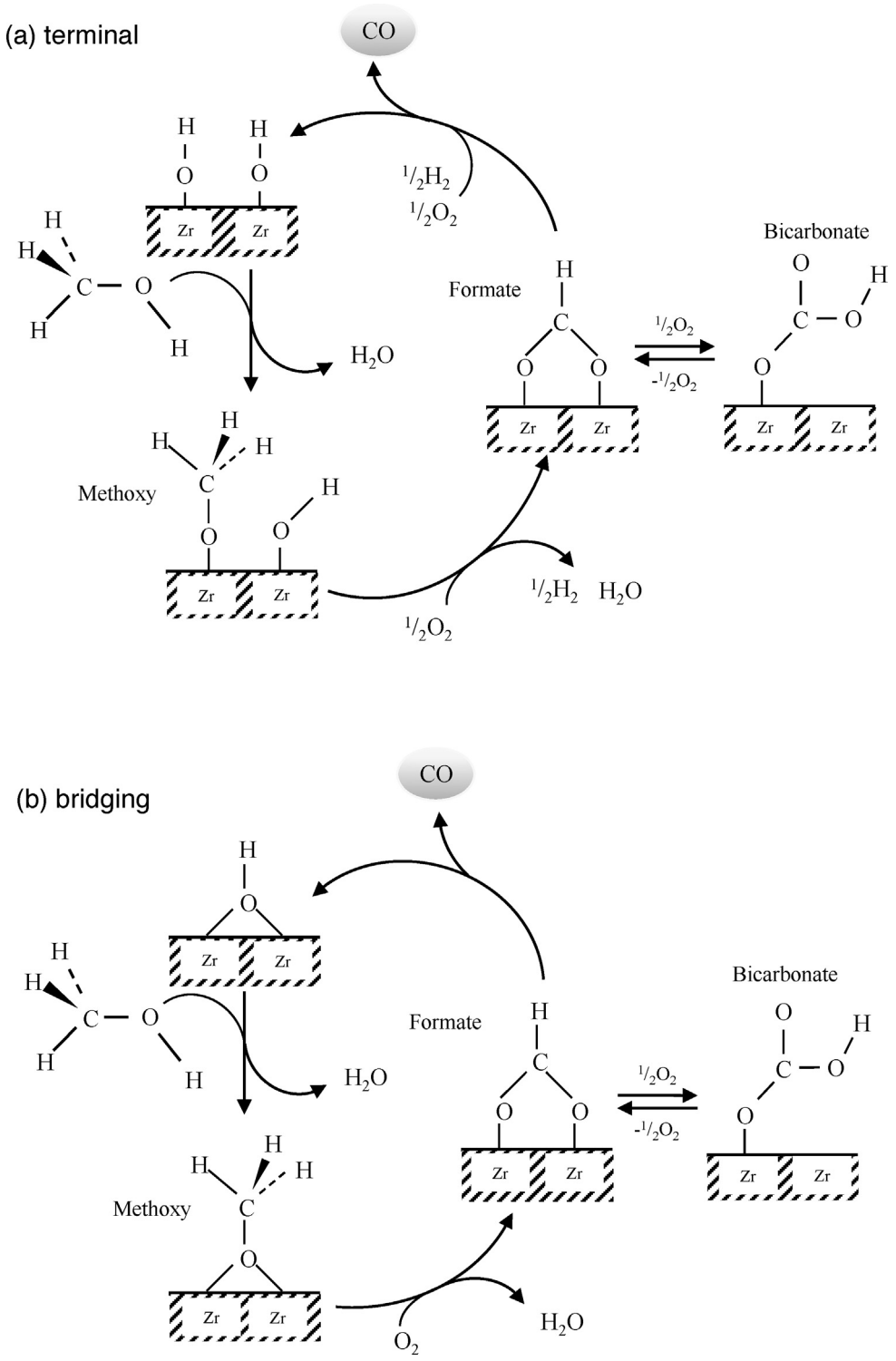

Fig. 10. Reaction mechanism over pure ZrO_2 for MeOH oxidation: (a) terminal type mechanism, (b) bridging type mechanism.

ing the measurement temperature increased from 200 °C to 300 °C, the methoxy species almost disappeared and the formate species maximized at 275 °C and then decreased at 300 °C. And noted that the large inverse bands appeared at 1150 cm^{-1} with increasing in the temperature to 300 °C. We suppose that this is attributed to desorption of some organic species contaminated in pure ZrO_2 as-obtained.

Next, *in situ* FT-IR analysis of the adsorption species during the MeOH oxidation over 2.0 wt% Ag/ZrO_2 (JRC-ZRO-3) at the temperature range of room temperature to 125 °C was also examined, as shown in Fig. 9. As a result, we observed one inverse band at around 3670 cm^{-1} associated with the bidentate hydroxyl groups, the adsorption bands attributed to methoxy species appeared at 2925 cm^{-1}, 2810 cm^{-1}, 1457 cm^{-1}, and 1195 cm^{-1}, and the bands to formate species appeared at 2870 cm^{-1}, 1573 cm^{-1}, 1384 cm^{-1}, and 1359 cm^{-1}. These results prove the adsorption of methoxy species on the ZrO_2 surface as with the case of pure ZrO_2. With an increase in the temperature, the inverse band assigned to

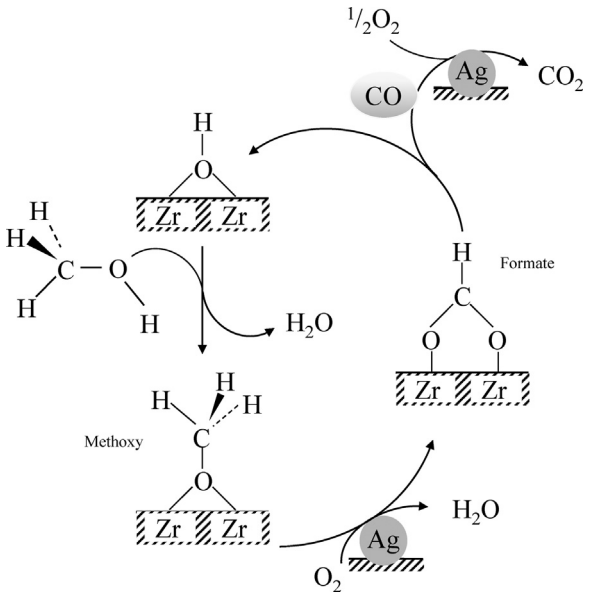

Fig. 11. Reaction mechanism over Ag/ZrO_2 for MeOH oxidation.

hydroxyl groups decreased gradually, indicating the regeneration of the hydroxyl groups by the progress of MeOH oxidation. In addition, it was observed that the formate species increased along with a decrease in the methoxy species. When the measurement temperature increased furthermore, the methoxy species almost disappeared at 125 °C and the formate species increased at once and then decreased slightly.

3.5. *Proposing the reaction mechanism of MeOH oxidation over Ag/ZrO_2*

Based on the FT-IR analysis and the activity test results, we have deduced the reaction mechanism of the MeOH oxidation on the pure ZrO_2 and Ag/ZrO_2. In the literature, the reaction mechanism of MeOH oxidation on CeO_2 and also Au/CeO_2 was reported by Rousseau et al. [17]. In addition, that of MeOH decomposition over Cu/ZrO_2 was also reported by Tsoncheva et al. [29]. We thus consider that the similar reaction occurs on ZrO_2 and Ag/ZrO_2.

In the case of pure ZrO_2, two types mechanism are considered as shown in Fig. 10. This is because that terminal and bridging hydroxyl groups were consumed by the adsorption of MeOH as shown in Fig. 8. With an increase in the reaction temperature, methoxy species are considered to be oxidized to formate species. It should be noted that this formate species can be easily transformed to bicarbonate species. When the reaction temperature increases furthermore, formate and bicarbonate species are decomposed to CO and the hydroxyl species for each type mechanism. The oxidation rate of methoxy species to formate species are slow below 250 °C, leading to the low activity of pure ZrO_2 for MeOH oxidation as shown in Fig. 1.

Regarding the effect of Ag on the catalytic oxidation reaction, several studies were reported, especially for the soot oxidation [45–47]. Aneggi et al. reported the high catalytic activity of Ag/ZrO_2 comparable to Ag/CeO_2 for soot oxidation, and also Nanba et al. revealed the presence of active oxygen species on Ag species for soot oxidation over Ag/ZrO_2 by analysis of temperature-programmed reduction by NH_3 (NH_3-TPR). For the case of MeOH oxidation over Ag/ZrO_2, the adsorption site of MeOH is considered to be only the bidentate hydroxyl groups on the ZrO_2 surface as shown in Fig. 11. The adsorbed methoxy species are easily oxidized to only the formate species, and then the formate species are decomposed to CO and the hydroxyl species. Here, the formed CO can be completely oxidized to CO_2 by the catalytic effect of the Ag component in a manner similar to the soot oxidation over Ag/ZrO_2 as mentioned above. In addition, Ag component can enhances the oxidation rate of methoxy species to formate species. Namely, we deduce that these assist of Ag component for two steps leads to the improvement of catalytic activity of Ag/ZrO_2 for MeOH oxidation.

It is well known that the CeO_2 based noble metal catalyst possesses the large OSC and its large OSC leads to the high catalytic activity for several oxidation reaction [38,48,49]. For the MeOH oxidation process, the Ag/ZrO_2 catalyst exhibits excellent activity comparable to the Ag/CeO_2 catalyst due to the significant effect of Ag component as an activator of oxygen molecular as revealed in the present work. Therefore, there is a possibility that Ag/ZrO_2 becomes a substitute material to CeO_2 supported various metal catalysts and it is also considerably attractive from the perspective of material cost.

4. Conclusions

Ag/ZrO_2 prepared by the impregnation method exhibited excellent activity comparable to Ag/CeO_2 for MeOH oxidative decomposition. The most active catalyst was 5.0 wt.% Ag catalyst supported on tetragonal ZrO_2 (JRC-ZRO-3) which was calcined at 500 °C. According to *in-situ* FT-IR study, we found that the adsorption sites of methanol are hydroxyl groups on the ZrO_2 surface. In addition, the formations of methoxy and formate and bicarbonate groups were observed as intermediate species. We thus conclude that Ag component enhances the oxidation step of methoxy species to formate species and CO formed by decomposition of formate species to CO_2, leading to the complete oxidation of MeOH over the Ag-based catalyst. The oxygen species mainly and effectively used for MeOH oxidation is considered an active oxygen species adsorbed and activated by the Ag component.

Acknowledgment

This study was supported by the Cooperative Research Program of Catalysis Research Center, Hokkaido University (Grant 14B1009).

References

[1] R. Atkinson, J. Arey, Chem. Rev. 103 (2003) 4605–4638.
[2] R. Atkinson, Atmos. Environ. 34 (2000) 2063–2101.
[3] B.J. Finlayson-Pitts, J.N. Pitts Jr., Science 276 (1997) 1045–1051.
[4] A. Guenther, C.N. Hewitt, D. Erickson, R. Fall, C. Geron, T. Graedel, P. Harley, L. Klinger, M. Lerdau, W.A. Mckay, T. Pierce, B. Scholes, R. Steinbrecher, R. Tallamraju, J. Taylor, P. Zimmerman, J. Geophys. Res. 100 (1995) 8873–8892.
[5] C. Yrieix, A. Dulaurent, C. Laffargue, F. Maupetit, T. Pacary, E. Uhde, Chemoshpere 79 (2010) 414–419.
[6] K. Eguchi, H. Arai, Catal. Today 29 (1996) 379–386.
[7] C. Hu, Q. Zhu, Z. Jiang, Y. Zhang, Y. Wang, Microporous Mesoporous Mater. 113 (2008) 427–434.
[8] D. Delimaris, T. Ioannides, Appl. Catal. B: Environ. 84 (2008) 303–312.
[9] T. Tsoncheva, G. Issa, T. Blasco, M. Dimitrov, M. Popova, S. Hernandez, D. Kovacheva, G. Atanasova, J.M.L. Nieto, Appl. Catal. A: Gen. 453 (2013) 1–12.
[10] V.P. Santos, S.A.C. Carabineiro, P.B. Tavares, M.F.R. Pereira, J.J.M. Orfao, J.L. Figueiredo, Appl. Catal. B: Environ. 99 (2012) 198–205.
[11] S. Scirè, L.F. Liotta, Appl. Catal. B: Environ. 125 (2012) 222–246.
[12] W. Walerczyk, M. Zawadzki, Catal. Today 176 (2011) 159–162.
[13] J. Peng, S. Wang, Appl. Catal. B: Environ. 73 (2007) 282–291.
[14] Y. Luo, Y. Xiao, G. Cai, Y. Zheng, K. Wei, Fuel 93 (2012) 533–538.
[15] W. Li, H. Zhang, X. He, H. Liu, J. Energy Chem. 22 (2013) 512–516.
[16] H. Huang, W. Li, H. Liu, Catal. Today 183 (2012) 58–64.
[17] S. Rousseau, O. Marie, P. Bazin, M. Daturi, S. Verdier, V. Harle, J. Am. Chem. Soc. 132 (2010) 10832–10841.
[18] K. Kahler, M.C. Holz, M. Rohe, A.C. van Veen, M. Muhler, J. Catal. 299 (2013) 162–170.
[19] P. Kaminski, M. Ziolek, J. Catal. 312 (2014) 249–262.
[20] H.K. Plummer Jr., W.L.H. Watkins, H.S. Gandhi, Appl. Catal. 29 (1987) 261–283.
[21] H.B. Zhang, W. Wang, Z.T. Xiong, G.D. Lin, Stud. Surf. Sci. Catal. 130 (2000) 1547–1552.
[22] L. Lefferts, J.G. van Ommen, J.R.H. Ross, Appl. Catal. 31 (1987) 291–308.
[23] E.M. Cordi, J.L. Falconer, Appl. Catal. A: Gen. 151 (1997) 179–191.

[24] L. Mo, A.H. Wan, X. Zheng, C.T. Yeh, Catal. Today 148 (2009) 124–129.
[25] Y. Binyamin, G.E. Shter, V. Gelman, D. Avnir, G.S. Grader, Catal. Sci. Technol. 1 (2011) 1593–1599.
[26] I.A. Fisher, A.T. Bell, J. Catal. 184 (1999) 357–376.
[27] T. Tsoncheva, S. Areva, M. Dimitrov, D. Paneva, I. Mitov, M. Linden, C. Minchev, J. Mol. Catal. A: Chem. 246 (2006) 118–127.
[28] S.D. Lin, H. Cheng, T.C. Hsiao, J. Mol. Catal. A: Chem. 342–343 (2011) 35–40.
[29] T. Tsoncheva, I. Genova, M. Dimitrov, E. Sarcadi-Priboczki, A.M. Venezia, D. Kovacheva, N. Scotti, V. dal Santo, Appl. Catal. B. Environ. 165 (2015) 599–610.
[30] L.M. Gomez-Sainero, S. Damyanova, J.L.G. Fierro, Appl. Catal. A: Gen. 208 (2001) 63–75.
[31] G. St. Christoskova, M. Stoyanova, M. Georgieva, D. Mehandzhiev, Appl. Catal. A: Gen. 173 (1998) 95–99.
[32] G. St. Christoskova, M. Stoyanova, N. Danova, O. Argirov, Appl. Catal. A: Gen. 173 (1998) 101–105.
[33] Y. Zhao, Z. Qin, G. Wang, M. Dong, L. Huang, Z. Wu, W. Fan, J. Wang, Fuel 104 (2013) 22–27.
[34] M. Trejda, M. Ziolek, Y. Millot, K. Chalupka, M. Che, S. Dzwigaj, J. Catal. 281 (2011) 169–176.
[35] H. Golinska, P. Decyk, M. Ziolek, Catal. Today 169 (2011) 242–248.
[36] M.A. Smith, A. Zoelle, Y. Yang, R.M. Rioux, N.G. Hamilton, K. Amakawa, P.K. Nielsen, A. Trunschke, J. Catal. 312 (2014) 170–178.
[37] C. Larese, F.C. Galisteo, M.L. Granados, R. Mariscal, J.L.G. Fierro, P.S. Lambrou, A.M. Efstathiou, J. Catal. 226 (2004) 443–456.
[38] Y. Nagai, T. Hirabayashi, K. Dohmae, N. Takagi, T. Minami, H. Shinjoh, S. Matsumoto, J. Catal. 242 (8) (2006) 103–109.
[39] S. Scirè, S. Minicò, C. Crisafulli, C. Satriano, A. Pistone, Appl. Catal. B: Environ. 40 (2003) 43–49.
[40] S. Damyanova, M.L. Cubeiro, J.L.G. Fierro, J. Mol. Catal. A: Chem. 142 (1999) 85–100.
[41] D. Zeng, S. Liu, G. Wang, H. Chen, J. Xu, F. Deng, Catal. Lett. 143 (2013) 624–629.
[42] R. Bonelli, S. Albonetti, V. Morandi, L. Ortolani, P.M. Riccobene, S. Scire, S. Zacchini, Appl. Catal. A: Gen. 395 (2011) 10–18.
[43] B. de Rivas, J.I. Gutierrez-Ortiz, R. Lopez-Fonseca, J.R. Gonzalez-Velasco, Appl. Catal. A: Gen. 314 (2006) 54–63.
[44] N. Shimoda, D. Shoji, K. Tani, M. Fujiwara, K. Urasaki, R. Kikuchi, S. Sataokawa, Appl. Catal. B: Environ. 174–175 (2015) 486–495.
[45] K. Shimizu, H. Kawachi, A. Satsuma, Appl. Catal. B: Environ. 96 (2010) 169–175.
[46] E. Aneggi, J. Llorca, C. de Leitenburg, G. Dolcetti, A. Trovarelli, Appl. Catal. B: Environ. 91 (2009) 489–498.
[47] T. Nanba, S. Masukawa, A. Abe, J. Uchisawa, A. Obuchi, Appl. Catal. B: Environ. 123–124 (2012) 351–356.
[48] L. Katta, P. Sudarsanam, G. Thrimurthulu, B.M. Reddy, Appl. Catal. B: Environ. 101 (2010) 101–108.
[49] G. Avgouropoulos, T. Ioannides, Appl. Catal. A: Gen. 244 (2003) 155–167.